3

Modelling and Analysis of the Induction-Heating Converters

András Kelemen and Nimród Kutasi
Sapientia Hungarian University of Transylvania
Romania

1. Introduction

The aim of this chapter is the presentation of some aspects related to the modelling and analysis of the induction-heating load-resonant converters as components of the induction-heating equipments.
The induction-heating converters are used to produce a high-intensity alternative magnetic field in an inductor. The workpiece placed in the inductor is heated up by eddy-current losses produced by the magnetic field at a frequency defined by technological requirements (Rudnev et al., 2003).
The basic principles of power electronic converter modelling are presented with emphasis on the specific solutions that can be applied in case of load-resonant converters. Detailed description and modelling of the electromagnetic, thermal and metallurgical phenomena involved in the induction-heating process is behind the scope of this chapter.
Mathematical modelling of the induction-heating equipments means the representation of the physical behaviour of these systems by mathematical means.
Generally, modelling should be concentrated on the phenomena which are of interest for the solution of the given engineering problem. These phenomena can be labelled as "dominant behaviour". All the other phenomena which have no influence from the point of view of the given problem are regarded as "insignificant phenomena". For example, the parasitic circuit components like the parasitic capacitances of power transistors and the stray inductances of busbars have negligible influence on the power control characteristics of a low-frequency or medium-frequency induction-heating inverter, while their influence is very important from the point of view of the transistor switching losses.
The model should be as simple as possible, because a simple model yields better physical insight. For instance, in the model of the resonant load circuit used for converter analysis, an inductor for induction heating can almost always be modelled by a serial LR circuit with constant inductance and resistance. Variation of these parameters with the temperature of the workpiece and with the process (for example with the position of the workpiece in a scanning inductor) can be taken into account by defining a possible range of inductor parameters. The behaviour of the converter is normally verified for several sets of parameters from this range, but these are kept constant during the converter analysis.
The refinement of the model can be made if necessary after the basic phenomena have been clarified. Depending on the problem to be analyzed, one can decide to refine the existing model or to go for other simplified models. For instance, the analysis of the DC-link voltage

of an induction-heating converter can be performed using a detailed rectifier and filter model, with the inverter input represented by equivalent resistive loads corresponding to different operating states of the inverter. With the variation range of the DC-link voltage determined this way, the operation of the inverter can be studied using an ideal voltage source. While this approach is useful for defining the component stresses and clarifying basic phenomena concerning the operation of these two sides of the converter, it can be naive in case of the controller design. Due to the dynamic influence between the filter and the inverter and due to the presence of AC components in the rectified voltage, the complete model is needed for controller design.
In the following, several modelling procedures are presented, which form a set of useful tools for analysis of the induction-heating converters when they are used according to the concept of hierarchical (multilevel) modelling.

2. The hierarchical approach to resonant converter modelling

One of the basic ideas emerging from the above principles is that modelling of the induction-heating load-resonant converters has to be made in a *hierarchical* way (Mohan et al., 2002). This means that different methods and tools have to be used depending on the details of the phenomena into which we want to get insight. Each modelling method or simulation program has its advantages and limitations, which make it suitable for the analysis of some of the aspects of a converter's behaviour.
It should be clarified that modelling is always an iterative process, even if some modelling steps are usually substituted by a-priori knowledge about the converter. For instance, a certain operation mode of a converter is normally the result of a closed-loop (controlled) operation, which can be assessed by higher-level modelling, but knowledge about the existence of this mode and about the circumstances it creates can be used for lower-level analysis (for example calculation of the switching device losses in a certain mode of operation).
The hierarchical approach is closely related to the main results expected from the modelling and simulation of the induction-heating converters, which are:

- calculation of the stress on the power devices in different operating conditions;
- reliable understanding of the converter operation based on the waveforms of different circuit variables;
- determination of the steady-state and dynamic performance of the system.

Modelling methods and analysis tools suitable for obtaining these results are presented in the following, with detailed discussion of some methods that make possible the analysis of the induction-heating load-resonant converters at higher hierarchical levels.
In case of a low-level analysis the electrical devices and circuits are modelled in detail, while in case of higher-level analysis simplifying assumptions are introduced, which ignore some details, but which make it possible to concentrate on the behaviour of the system as a whole.
The computing effort is kept almost the same at different levels of the hierarchy at the expense of simplifying assumptions. At higher levels the detailed circuit models are replaced by behavioural ones.
Most knowledge about the converter operation can be obtained by dynamic modelling, which makes also possible the synthesis of the control system.
In case of the induction-heating converters the main control tasks are the control of the switching conditions and the control of the heating power.

The switching conditions are usually controlled by means of some PLL loop version. The task of this controller is either to assure some essential operating conditions (for example a capacitive phase shift between the output current and voltage of a current-source thyristor-based inverter) or to create optimal switching conditions (for example zero voltage switching in case of a transistor-based voltage inverter).
The power control is performed either by means of an auxiliary converter, or by means of the resonant inverter. The use of an auxiliary converter makes possible the decoupling of the two main control tasks (Kelemen & Kutasi, 2007a).
Examples for the use of auxiliary converters are the application of controlled rectifiers in case of medium frequency induction-heating converters with thyristor-based current inverter and the application of step-down DC-DC converters in case of the high-frequency voltage inverters with power control by pulse amplitude modulation.
The power control by means of the inverter can be performed in several ways including different pulse width modulation (PWM) methods, pulse density modulation (PDM) (Fujita & Akagi, 1996), frequency shift control (FS) and their different combinations (Kelemen, 2007).
Small-signal (linearized) models can be used successfully to design control loops relying on classical control theory, while large-signal (usually nonlinear) models can be used for controller design based on the nonlinear control theory.
Sometimes the delay introduced by the processing time of the controller should also be modelled. Thus, the presence of the controller itself becomes an input data for the controller design.
Detailed modelling is generally used to determine the stress on the power devices and for detailed analysis of the high-speed processes, like transistor switching. Such high-speed processes are strongly influenced by circuit components like snubbers, which do not influence the main behaviour of the converter.
This level of the detailed analysis can be performed using general-purpose simulation programs, which solve in each step of the simulation a complicated nonlinear system of equations. The detailed modelling approach can be problematic due to the large scale of the time constants of the processes involved. Due to the fast variation of the circuit variables during switching, it can happen that the initial guess used in the corresponding time step is not close enough to the solution to assure the convergence of the solver.
Besides, for an acceptable computing time it is important to set the initial conditions of the whole simulation close to the steady-state values of the state variables.
These values can be obtained using a less detailed analysis based for instance on a **switched-circuit model**, which contains only the main circuit components and which can be used to determine the dominant circuit waveforms. This kind of model can offer insight into the principles of the converter operation, but handling of the switches needs special techniques.
Switched-circuit models can be built based either on ideal or on non-ideal switches. Non-ideal power electronic switches are often represented as piece-wise linear networks.
The main problems to be solved are:

- the switching instants of "internally controlled" switches have to be determined accurately;
- switching can cause discontinuity of the state variables of the circuit (Dirac pulses);
- the circuit topology subsequent to the switching has to be determined correctly;
- the initial conditions of a switching state have to be determined in a "consistent" way, i.e. given the solution of the circuit immediately before the switching instant, the solution in the moment immediately following the switching instant has to be determined.

Not surprisingly, the switched-circuit modelling with ideal switches is similar to the approach used in case of the **hybrid systems**, a class of systems which nowadays represents the subject of intense research activity.
The load-resonant induction-heating inverters are inherently hybrid systems consisting of circuits with continuous dynamics and of switching devices. Hybrid modelling and analysis is a powerful tool for describing the behaviour of the system.
The key problem is to model the discrete transitions (when and how) and to associate to each discrete state a corresponding continuous dynamics. To address this problem one can use the hybrid automaton theory (Torrisi & Bemporad, 2004), (Borelli, 2003).
In the following the idea of hybrid modelling is outlined in case of the induction-heating voltage inverter with LLC resonant load (Fig. 1).

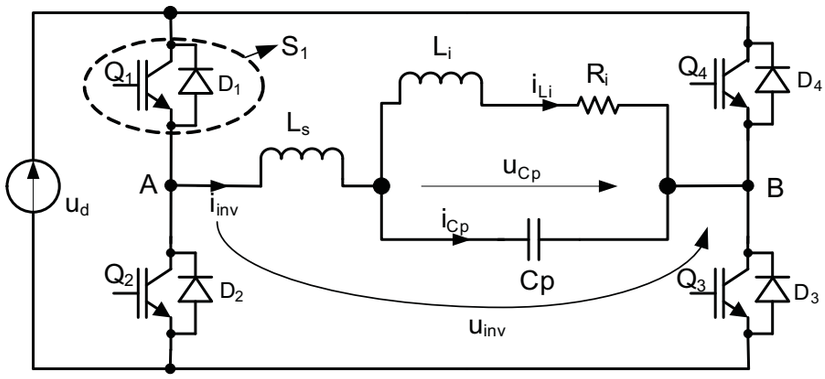

Fig. 1. Voltage inverter with LLC resonant load

Let $X \in \Re^n$ be the continuous space of the inverter states and let $Q \in \{q_1, q_2, \ldots, q_m\}$ be a finite set of discrete states. In case of the inverter from Fig. 1 and the control strategy presented below, n=3 and m=3. The continuous state space specifies the possible values of the continuous states for all switching configurations $q \in Q$ of the converter. For each $q \in Q$ the continuous dynamics can be modelled by differential equations of the form:

$$\dot{\underline{x}}(t) = f_q(\underline{x}(t)) = A_q \cdot \underline{x}(t) + b_q ; \quad A_q \in \Re^{n \times n}, b_q \in \Re^{n \times 1}, \underline{x} \in X . \tag{1}$$

The states of the circuit from Fig. 1 are: $\underline{x}(t) = \left[i_{inv} \quad i_{Li} \quad u_{Cp} \right]^T$. The discrete states of the system are defined by the states of the two-quadrant switches *S1, S2, S3* and *S4*. Each of the switches consists of a transistor Q_i and its anti-parallel diode D_i. The transistors are turned on and off by gate control, while the diodes are controlled by their currents and AK voltages. There are several possible strategies for the control of the inverter from Fig. 1 (Kelemen, 2007). A possible sequence of the gate control signals is shown in Fig. 2 along with characteristic waveforms of the i_{inv} inverter current and of the u_{Cp} capacitor voltage. This control mode is characterized by three discrete states (2) and is called *discontinuous current mode* due to the existence of the state q_3.

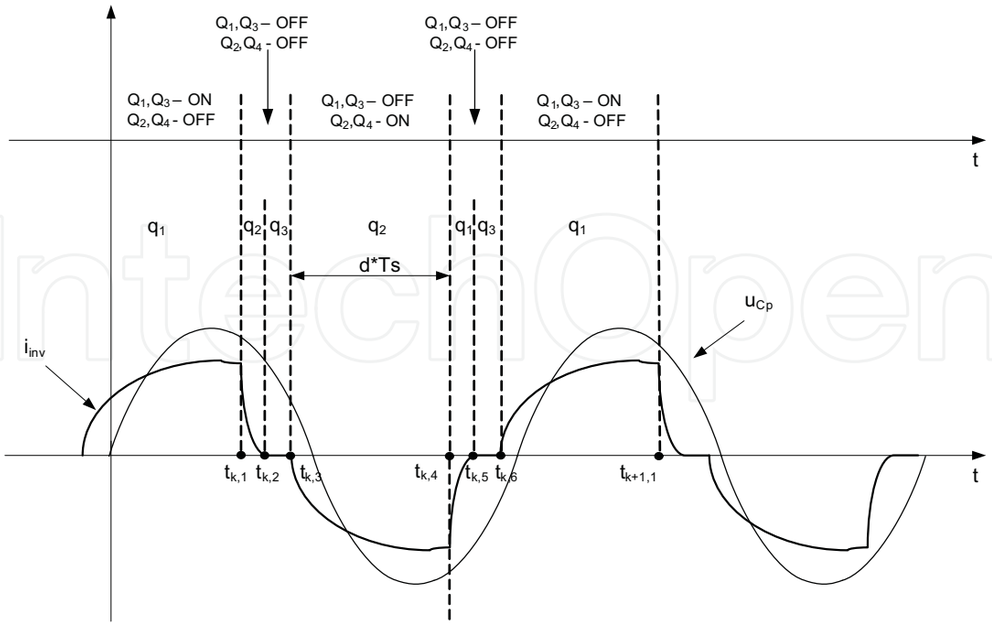

Fig. 2. The resonant load capacitor voltage u_{Cp} and the inverter output current i_{inv} in discontinuous current operation mode

$$\begin{aligned} q_1 &= \left(S_1 - ON, S_3 - ON, S_2 - OFF, S_4 - OFF\right) \\ q_2 &= \left(S_1 - OFF, S_3 - OFF, S_2 - ON, S_4 - ON\right) \\ q_3 &= \left(S_1 - OFF, S_3 - OFF, S_2 - OFF, S_4 - OFF\right) \end{aligned} \quad . \tag{2}$$

The transitions between the different discrete states are related to the time instances denoted by $t_{k,i}$. For instance the first discrete state q_1, characterized by the conduction of Q_1 and Q_3, is followed from the moment $t_{k,1}$ by the state q_2, characterized by the conduction of the diodes D_2 and D_4. The third discrete state means that all switches are open, no transistor or diode is in conduction, and consequently the inverter output current is interrupted.

The hybrid model of the system is depicted in Fig. 3. The hybrid automaton H has been decomposed in two hybrid automata H_1 and H_2. H_1 is a finite state machine governing the discrete transitions which depend on the continuous state vector $\underline{x}$ delivered by H_2. The continuous states $\underline{x}$ of H_2 evolve according to the discrete variable $\delta \in \Delta$ ($\Delta = \{\delta_1, \delta_2, \delta_3\}$) received from H_1. The discrete transitions are governed by the time instances determined by the controllers and by the internal switching conditions. The linear circuits with continuous dynamics corresponding to the discrete states are also shown in Fig. 3.

Fig. 4 presents the structure of the inverter controller, indicating the influence of its components on the different switching instances. Thus, $t_{k,1}$ and $t_{k,4}$ are determined by the frequency controller and the voltage-controlled oscillator (VCO), while $t_{k,2}$ and $t_{k,5}$ are determined by the voltage (power) controller.

The uncontrolled ("internally controlled", "indirectly controlled") switching instances $t_{k,3}$ and $t_{k,6}$ depend on the parameters of the resonant load and on the DC supply voltage.

The hybrid automaton H can be transformed into different models (PWA – **P**iece-**W**ise **A**ffine, DHA – **D**iscrete **H**ybrid **A**utomaton) for analysis and controller design using high-level hybrid-system describing languages like HYSDEL (Torrisi & Bemporad, 2004).

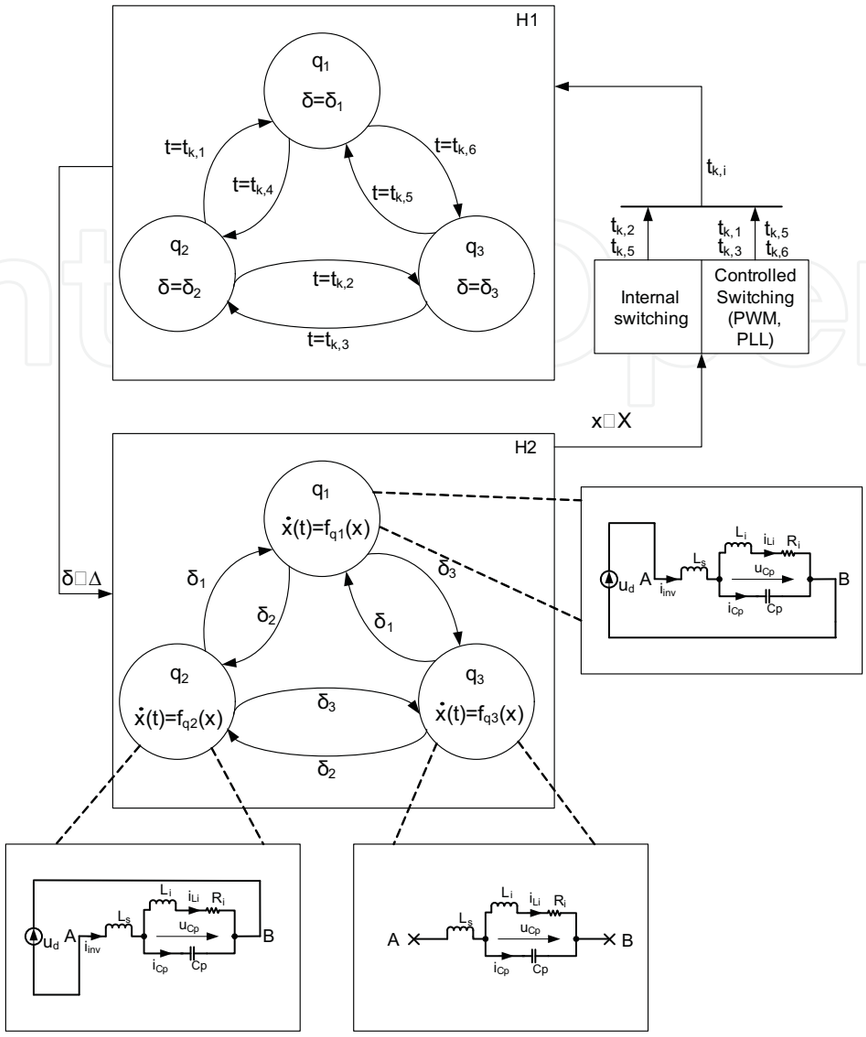

Fig. 3. The hybrid model of the inverter with LLC resonant load in discontinuous current mode of operation

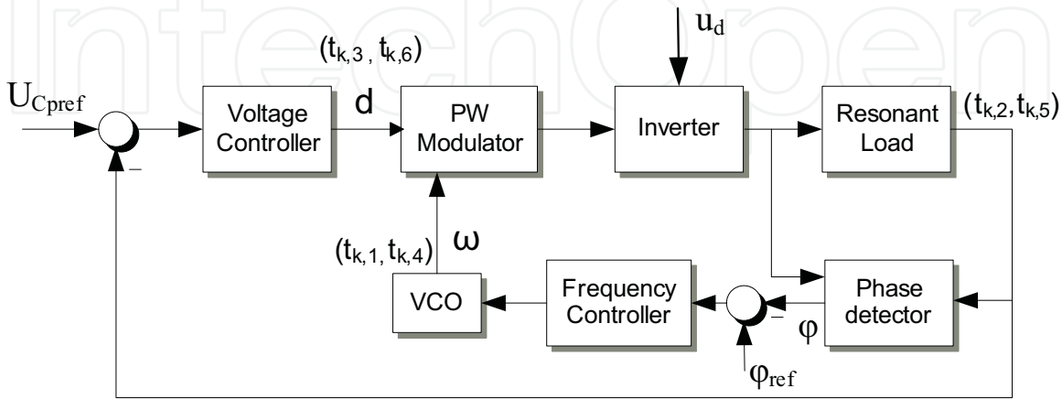

Fig. 4. The principle of closed-loop control of the inverter with LLC resonant load in discontinuous current operation mode

Taking into account the hybrid nature of the power electronic converters, we can say that the hybrid modelling and analysing approach is the natural way in this field.
A further step towards the simplification of the converter model can be made by **averaging** performed either over the state-space equations or directly over the converter circuit. In case of the resonant converters, the simulation of the closed-loop, large-signal behaviour is a challenge due to the high-frequency large variation of the state variables, which makes the state-space averaging method useless. Due to large variation of the state variables within a switching cycle, the state-space averaging method would pass over the essential phenomena.
The averaging method has been generalized in order to be applicable also in case of resonant converters. Application examples of the classical and generalized averaging methods are given in the next subsections, with detailed presentation of the *d-q* modelling technique.
In order to avoid the need to model the high-frequency variations of the state variables, the **sampled-data modelling technique** has been proposed for description of both large-signal and small-signal dynamics of resonant converters (Elbuluk et al., 1998). In this case, the states of the converter are redefined to be equal with their values at the ends of the switching periods.

3. Modelling of the induction-heating resonant load circuit

The induction-heating resonant load is composed of usually linear and time-invariable reactive components and the induction-heating inductor. The structure of the resonant load is strongly dependent on the induction-heating converter topology and the load either can be viewed as power-factor compensation scheme, or can be considered a component of the load-resonant converter.
The description of the inductor's behaviour is a coupled-field problem, with electromagnetic, thermal, metallurgical and hydrodynamic phenomena with more or less strong coupling.
For instance, the temperature of the workpiece has a strong influence on the electromagnetic phenomena, like the penetration depth and the power density. This influence becomes strongly non-linear when the metallurgical phase transformation leads to a sudden change of the magnetic properties of the workpiece at the Curie temperature.
The induction heating represents a transient process both from thermal and electromagnetic point of view, but the behaviour of the electric circuit is usually analysed assuming a permanent thermal state.
For a given operating frequency and temperature distribution, the inductor and the workpiece can be represented by an equivalent RL circuit.
Usually, the quality factor of the inductor is 3...40 ($\cos\varphi < 0.4$), with lower values in case of inductors with field concentrators and higher values in case of weak coupling between the inductor and the load (ex. vacuum melting). The equivalent parameters are valid only for a given intensity of the magnetic field. In the simple case of a cylindrical workpiece in a long inductor, the equivalent impedance has the form (3) (Sluhotkii & Rîskin, 1982).

$$\underline{Z_e} = a\sqrt{f} + j\left(b\sqrt{f} + cf\right). \tag{3}$$

In case of strong coupling and large variation of the operating frequency, a "large bandwidth" model can be used (Forest et al., 2000) in order to take into account the frequency-dependence of the equivalent parameters (Fig. 5).

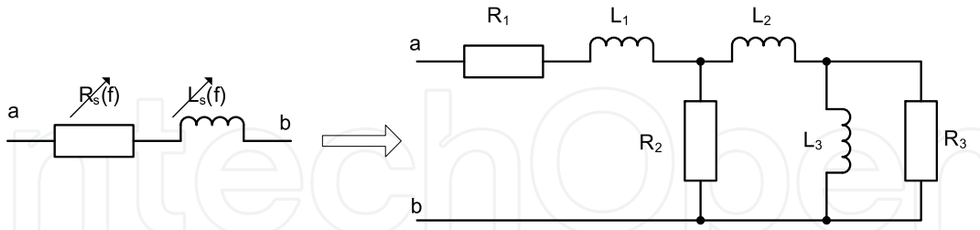

Fig. 5. Serial RL inductor model with frequency-dependent parameters and its large-bandwidth equivalent circuit with constant parameters

4. Converter modelling by averaging techniques

A popular class of analysis methods for power electronic converters is based on the **averaging technique**. Different versions of this technique have been developed based on assumptions fulfilled by different classes of converters and these methods can provide large-signal (nonlinear) and small-signal (linear) converter models.

In fact, averaging represents a kind of transformation, which replaces the original "fast" variables with "slow" variables. For instance, the evolution in time of the inductor current from a step-down DC-DC converter can be seen as the evolution of the DC component of this current, with a superimposed ripple. The DC component means in fact the moving average, with slow variation.

The question can be raised whether the trajectory of this moving average is represented well enough by the trajectory of the corresponding quantity from the averaged model, and which are the conditions that must be satisfied in order to have a good approximation of the converter operation? (Krein et al., 1990). There are also questions, whether the averaged model is valid for large variations of the signals and whether stability properties of the system are preserved by the transformation, or not.

Periodically driven systems, like the power-electronic converters can be modelled using the **generalized averaging** method, presented in (Sanders et al., 1991).

The generalized averaging concept is based on the calculation of the time-dependent complex Fourier coefficients of the circuit variables, using a sliding frame equal with a switching period.

For a system-level analysis the circuit variables can be represented with acceptable accuracy by the first one or two terms of their Fourier series expansion. For instance, in case of a switch-mode DC-DC converter, the evolution of the average output voltage (i.e. of the first Fourier term) is important from the point of view of the controller design, while in case of a load-resonant induction-heating inverter, the amplitude of the resonant capacitor voltage (i.e. the second term) is of interest.

For a circuit variable x, the coefficients of the series (4) are defined by (5) (Sanders et al., 1991).

$$x(t-T+\tau)=\sum_{k}\langle x\rangle_{k}(t)e^{jk\omega(t-T+\tau)} \tag{4}$$

$$\langle x\rangle_k(t)=\frac{1}{T}\int_0^T x(t-T+\tau)e^{-jk\omega(t-T+\tau)}d\tau \tag{5}$$

T is the switching period, $\omega=2\pi/T$ and τ is the time from the beginning of the sliding frame.

The question is how do the Fourier coefficients vary with time if the circuit variables satisfy a given set of differential equations (6).

$$\frac{d}{dt}\underline{x}=f(\underline{x},\underline{u}) \tag{6}$$

In (5) $\underline{x}$ is the state vector and $\underline{u}$ is the periodic input of the system.

After expansion of (6), imposing the equality of the corresponding coefficients, it results:

$$\left\langle \frac{d}{dt}\underline{x}\right\rangle_k=\left\langle f(\underline{x},\underline{u})\right\rangle_k \tag{7}$$

Using the differentiation rule (8)

$$\frac{d}{dt}\langle\underline{x}\rangle_k=\left\langle \frac{d}{dt}\underline{x}\right\rangle_k-jk\omega\langle x\rangle_k, \tag{8}$$

the relation (7) becomes:

$$\frac{d}{dt}\langle\underline{x}\rangle_k=-jk\omega\langle x\rangle_k+\left\langle f(\underline{x},\underline{u})\right\rangle_k. \tag{9}$$

This differential equation doesn't contain the *k*-th order high-frequency terms. Instead, by means of the Fourier coefficients, it describes the "slow" variation of the amplitude of the state variables.

This method is similar to the time-varying phasor analysis presented in (Rim & Cho, 1990), which introduces a modified phasor $\underline{X(t)}$, defined by:

$$x(t)\equiv \mathrm{Re}\left\{\sqrt{2}\,\underline{X(t)}e^{j\omega t}\right\}. \tag{10}$$

In (10), $x(t)$ represents a sinusoidal function of time with slowly varying amplitude.

Substituting $k=0$ into (9) the result is the well-known **state-space averaging** method introduced by Cuk and Middlebrook in 1977, which can be used to describe the operation of hard-switching PWM DC-DC converters, but it is not suitable for analysis of quasi-resonant or resonant converters.

For steady-state analysis of the resonant converters, the so-called "cyclic-averaging" technique is useful (Foster et al., 2003).

In subsections 4.1 and 4.2 it is demonstrated, how the averaging techniques can be applied for modelling of the induction-heating converters. First the *d-q* modelling method (Zhang & Sen, 2004) is applied as a version of generalized averaging in order to build an inverter model which can be used for the design of the PLL and power controllers.

In the case presented in subsection 4.1 the power is controlled by means of the inverter.
In the case of the converter presented in subsection 4.2, the power control is solved by an auxiliary converter, which is modelled using the state-space averaging method.

4.1. The *d-q* model of a voltage inverter with LLC resonant load

The resonant inverter with hybrid LLC load and its characteristic waveforms are presented in Fig. 6 (Kelemen & Kutasi, 2007a). This load matching solution is also called "resonance transformation" (Fischer & Doht, 1994).

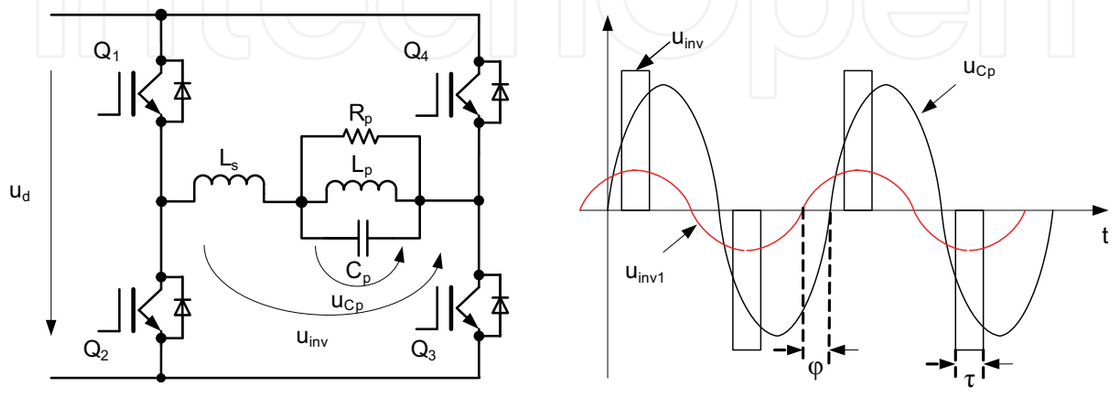

a) b)

Fig. 6. Voltage inverter, a) with LLC resonant load and parallel inductor model and b) its characteristic waveforms

The complex circuit of the resonant inverter is composed from the original and its orthogonal circuit (Fig. 7). Fig. 8 shows the high-frequency complex circuit variables expressed in *d-q* form.
Substituting the complex current of the L_s inductor into the inductor voltage equation, it results:

$$\underline{u}_{Ls}(t) = \left(u_{Lsd}(t) + ju_{Lsq}(t) \right) e^{j\omega t} = L_s \left(\frac{d}{dt} \left(i_{Lsd}(t) + ji_{Lsq}(t) \right) + j\omega \left(i_{Lsd}(t) + ji_{Lsq}(t) \right) \right) e^{j\omega t} . \quad (11)$$

The complex current of capacitor C_p results from the complex capacitor voltage as

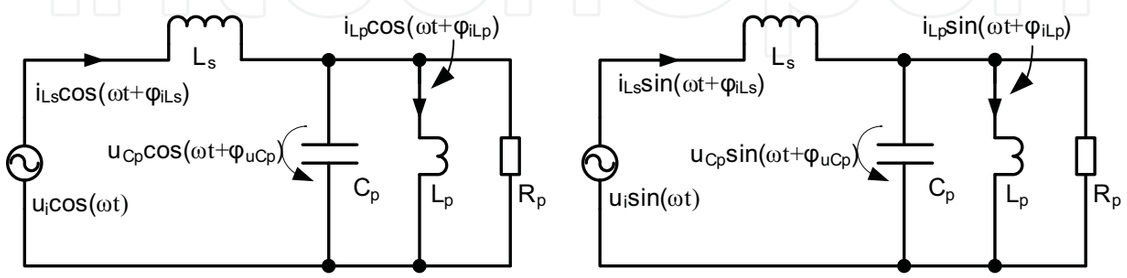

a) b)

Fig. 7. The inverter with resonant load and its orthogonal circuit

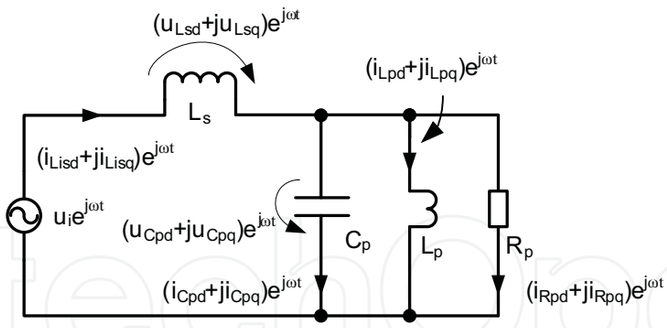

Fig. 8. The complex inverter circuit

$$\underline{i}_{Cp}(t) = \left(i_{Cpd}(t) + ji_{Cpq}(t)\right) e^{j\omega t} = C_p\left(\frac{d}{dt} + j\omega\right)\left(u_{Cpd}(t) + ju_{Cpq}(t)\right) e^{j\omega t}. \tag{12}$$

Assuming low-frequency variation, thus negligible second derivative of $u_{Cpd}(t)$ and $u_{Cpq}(t)$, the current of the inductor L_p can be expressed as follows:

$$\underline{i}_{Lp}(t) = \frac{1}{L_p}\int\left(u_{Cpd} + ju_{Cpq}\right) e^{j\omega t} = \frac{1}{\omega L_p}\left(\frac{1}{\omega}\frac{d}{dt} - j\right)\left(u_{Cpd} + ju_{Cpq}\right) e^{j\omega t}. \tag{13}$$

After removal of the high-frequency terms from (11), (12) and (13), the corresponding relations can be modelled with passive circuit components and controlled voltage or current sources. The low-frequency complex *d-q* model is obtained (Fig. 9), with low-frequency complex circuit variables, the time-dependence of which has not been shown for simplicity of notation. Decomposition of the complex *d-q* model leads to the low-frequency *d-q* model from Fig. 10.

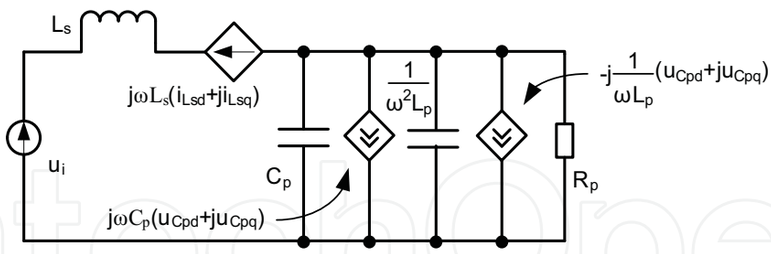

Fig. 9. Low-frequency complex d-q model of the resonant inverter

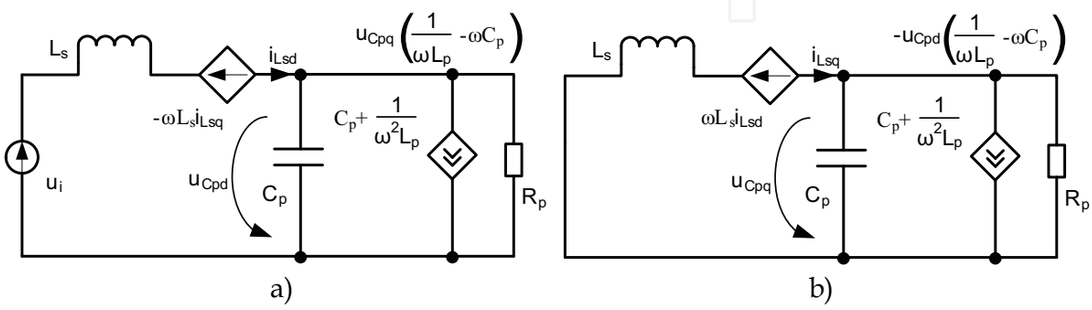

Fig. 10. Low-frequency d (a) and q (b) circuits

Start-up evolution of the resonant capacitor tank voltage under various load conditions is shown in Fig. 11.a. The circuit parameters of the resonant tank are $C_p = 63\ \mu F$, $L_s = 20\ \mu H$ and $L_p = 4\ \mu H$. The resonant capacitor tank voltage is controlled by means of pulse width modulation of the inverter output voltage, while the phase shift φ is controlled by a phase locked loop. Start-up evolution of the phase shift φ is shown in Fig. 11.b. The initial duty factor, the start-up frequency and the controller coefficients are $D_{start} = 0.005$, $f_{start} = 15$ kHz, $K_1 = 0.005$, $K_2 = 0.3$, $K_3 = 1000$, $K_4 = 50K_3$, while the voltage and phase shift set-values are $U_{Cpref} = 300\ V$ and $\varphi_{ref} = 50^\circ$. Unstable operation can be observed in case of a high quality factor.

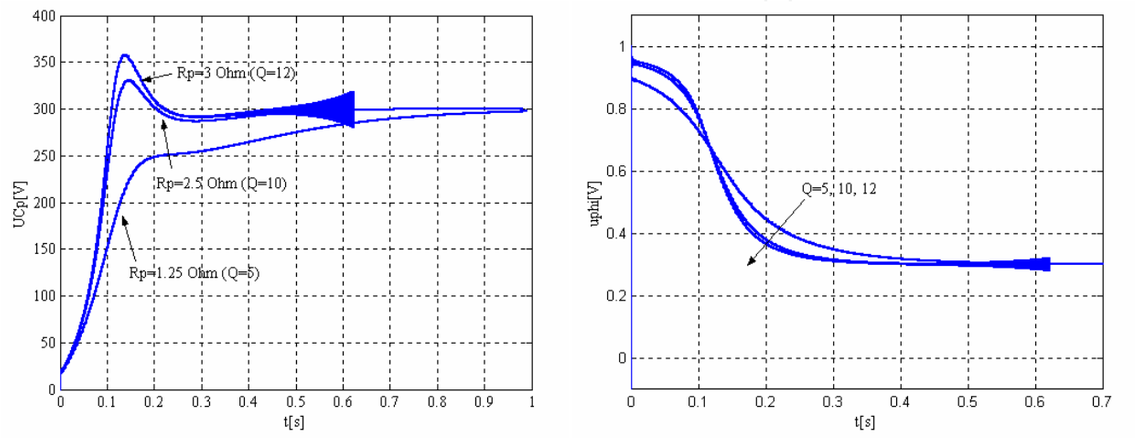

a) b)

Fig. 11. Start-up evolution of the resonant capacitor tank voltage u_{Cp} (a), and of the phase shift φ (u_{phi} is the output voltage of the phase detector, 0.5 V corresponding to $\varphi = 90^\circ$), for different values of the quality factor (Q = 5, 10, 12)

The small-signal model resulting from the perturbation of the above *d-q* model is shown in Fig. 12. The steady-state *d-q* components of the state variables and of the angular frequency are denoted with I_{Lsd}, I_{Lsq}, U_{Cpd}, U_{Cpq} and Ω.

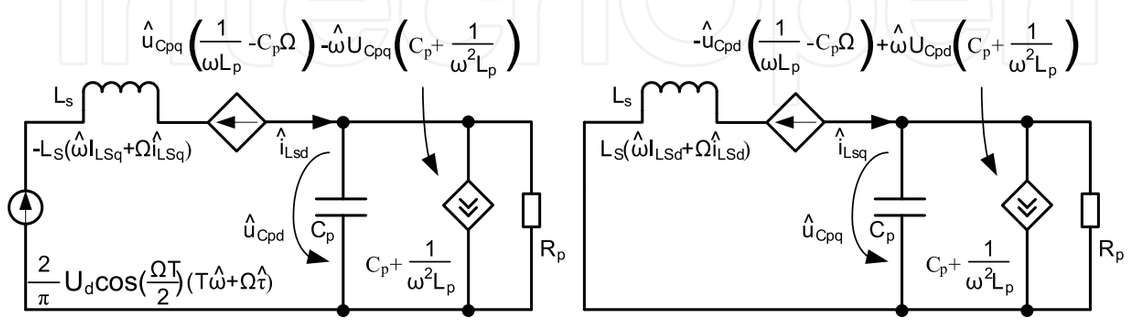

Fig. 12. Small-signal low-frequency d-q model of the inverter with LLC resonant load and parallel equivalent inductor circuit

4.2. State space averaging in case of a converter with pulse amplitude modulation

State-space averaging is an efficient method for analysis of converters characterized by the fulfilment of certain simplifying conditions. These are generally formulated as the small ripple condition and the linear ripple approximation (Erickson & Maksimović, 2004), (Sanders et al., 1991).

Small ripple means that the DC component of the signal for which this condition is applied is much larger than the other terms of its Fourier expansion. Of course the meaning of "much larger" is not easy to be defined and only the accuracy of the final result can tell whether its interpretation had been correct or not.

An application example of the state-space averaging can be given for the induction-heating converter with voltage inverter fed from a two-quadrant DC-DC converter (Fig. 13). In this case this intermediary converter solves the modulation of the DC voltage, providing the power control by pulse amplitude modulation.

The output voltage of this step-down DC-DC converter can always be handled from the point of view of the converter analysis as a small-ripple signal. This is simply the requirement from the load side and the converter must be designed to have a small output voltage ripple. The result is that the output voltage can be considered a DC voltage from the point of view of its influence on other circuit variables. Knowledge of the circuit variables determined by the consequently simplified analysis further gives the possibility to determine the small ripple itself.

The linear ripple approximation means that the given signal is assumed to have a linear variation during a switching state of the converter. This is the case of the inductor current from the two-quadrant DC-DC converter used to supply the induction-heating inverter with pulse amplitude modulation from Fig. 13.

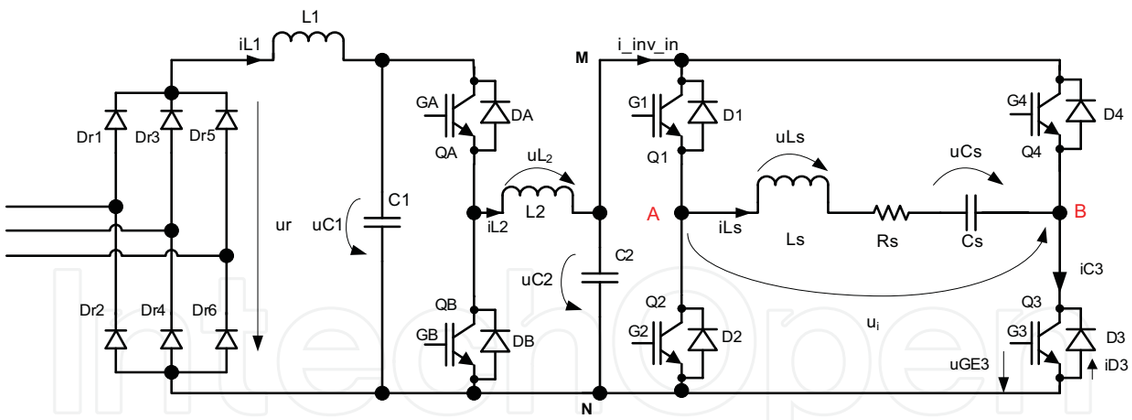

Fig. 13. Induction-heating converter with power control by pulse amplitude modulation

Let us consider the variation of the inductor current over a switching period. The switching states are:

$$q_1 = \left(Q_A - ON, Q_3 - OFF\right) and\ q_2 = \left(Q_A - OFF, Q_3 - ON\right). \tag{14}$$

The u_{L2} inductor voltage is assumed to be approximately constant during a switching period i.e. $u_1(t) = u_{L2\_q1} = u_{C1}(t) - u_{C2}(t) \cong ct.$ and $u_1(t) = u_{L2\_q1} = u_{C1}(t) - u_{C2}(t) \cong ct.$.

Thus, the inductor current has linear variation in each switching state i.e. it satisfies the linear ripple condition (Fig. 14).

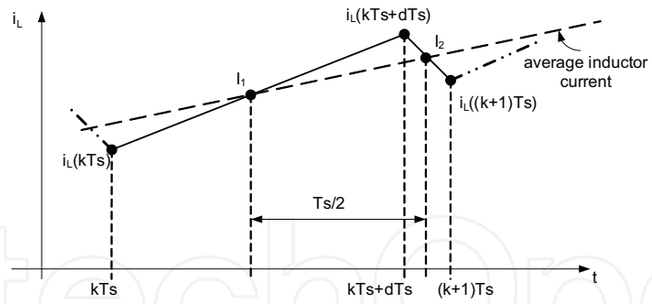

Fig. 14. Variation of the instantaneous and average inductor current in a step-down converter

Consequently:

$$\left(i_L((k+1)\cdot T_s)-i_L(k\cdot T_s)\right)/T_s = d\cdot\left\langle u_1(t)\right\rangle_{dT_s}+(1-d)\cdot\left\langle u_2(t)\right\rangle_{(1-d)T_s} = d\cdot u_1(t)+(1-d)\cdot u_2(t) \tag{15}$$

It results, that the average variation of the current is equal to the weighted sum of the inductor voltages (the weights are defined by the duty factor, which has a slow variation with time).
The variation of the average current can be found as follows (Fig. 14):

$$\frac{d\left\langle i_L(t)\right\rangle_{T_s}}{dt} = \frac{I_2-I_1}{T_s/2} = \frac{i_L((k+1)\cdot T_s)-i_L(k\cdot T_s)}{T_s}\,. \tag{16}$$

From (15) and (16) it results, that

$$\frac{d\left\langle i_L(t)\right\rangle_{T_s}}{dt} = d\cdot u_1(t)+(1-d)\cdot u_2(t)\,, \tag{17}$$

which is a differential equation defined by the "slow" variables $\left\langle i_L(t)\right\rangle_{T_s}$, $u_1(t)$, $u_2(t)$ and called "averaged state-space equation".
The small-signal model is obtained by perturbing the steady-state values of the state variables and of the duty factor *d* according to (18).

$$x = X+\hat{x}\,,\ d = D+\hat{d}\,. \tag{18}$$

In case if the inverter from Fig. 13 is replaced by a resistive load *R* between points "M" and "N", the averaged state-space equations and the corresponding small-signal equations of the step-down converter are:

$$\begin{aligned}
&\frac{d\left\langle i_{L1}\right\rangle_{T_s}}{dt} = -\frac{1}{L_1}\left\langle u_{C1}\right\rangle_{T_s}+\frac{1}{L_1}\left\langle u_r\right\rangle_{T_s} \quad\Rightarrow\quad \frac{d\hat{i}_{L1}}{dt} = -\frac{1}{L_1}\hat{u}_{C1}+\frac{1}{L_1}\hat{u}_r\\
&\frac{d\left\langle u_{C1}\right\rangle_{T_s}}{dt} = \frac{1}{C_1}\left\langle i_{L1}\right\rangle_{T_s}-\frac{d}{C_1}\left\langle i_{L2}\right\rangle_{T_s} \quad\Rightarrow\quad \frac{d\hat{u}_{C1}}{dt} = \frac{1}{C_1}\hat{i}_{L1}-\frac{1}{C_1}D\hat{i}_{L2}-\frac{1}{C_1}\hat{d}I_{L2}\\
&\frac{d\left\langle i_{L2}\right\rangle_{T_s}}{dt} = \frac{d}{L_2}\left\langle u_{C1}\right\rangle_{T_s}-\frac{1}{L_2}\left\langle u_{C2}\right\rangle_{T_s} \quad\Rightarrow\quad \frac{d\hat{i}_{L2}}{dt} = \frac{1}{L_2}D\hat{u}_{C1}+\frac{1}{L_2}\hat{d}U_{C1}-\frac{1}{L_2}\hat{u}_{C2}\\
&\frac{d\left\langle u_{C2}\right\rangle_{T_s}}{dt} = \frac{1}{C_2}\left\langle i_{L2}\right\rangle_{T_s}-\frac{1}{RC_2}\left\langle u_{C2}\right\rangle_{T_s} \quad\Rightarrow\quad \frac{d\hat{u}_{C2}}{dt} = \frac{1}{C_2}\hat{i}_{L2}-\frac{1}{RC_2}\hat{u}_{C2}
\end{aligned}\,. \tag{19}$$

4.3. The model of the converter with pulse amplitude modulation

The small-signal model of the induction-heating converter from Fig. 13 with power control by means of pulse amplitude modulation (PAM) is built using the model of the step-down converter obtained by state-space averaging and the *d-q* model of the voltage inverter with serial resonant load. The small-signal inverter model for serial load is built using the procedures described in 4.1 for the case of the voltage inverter with hybrid LLC load.

This model is meant for controller design using the classical control theory. The controller design can also be made starting from a model with the DC-DC converter supplied from an ideal voltage source. Later the influence of the L_1C_1 (Fig. 13) input filter is taken into account using the Middlebrook's extra element theorem (Erickson & Maksimović, 2004), i.e. the condition can be established to have similar performances to those of the system with ideal voltage source.

The load of the step-down converter is modelled by a current source, controlled by the inverter output current. The inverter operates with rectangular output voltage and pulse amplitude modulation control is being considered.

For a given operating point of the converter, the duty factor D, the capacitor voltage components and amplitude U_{Csd}, U_{Csq} and U_{Cs}, which are parameters of the small-signal model, are known, respectively can be determined from the steady-state circuit equations.

The small-signal model of the system composed of filter, step-down converter, inverter and resonant load is shown in Fig. 15.

The block diagram of the controlled converter, built using the principle of superposition, is shown in Fig. 16 (Kelemen, 2007).

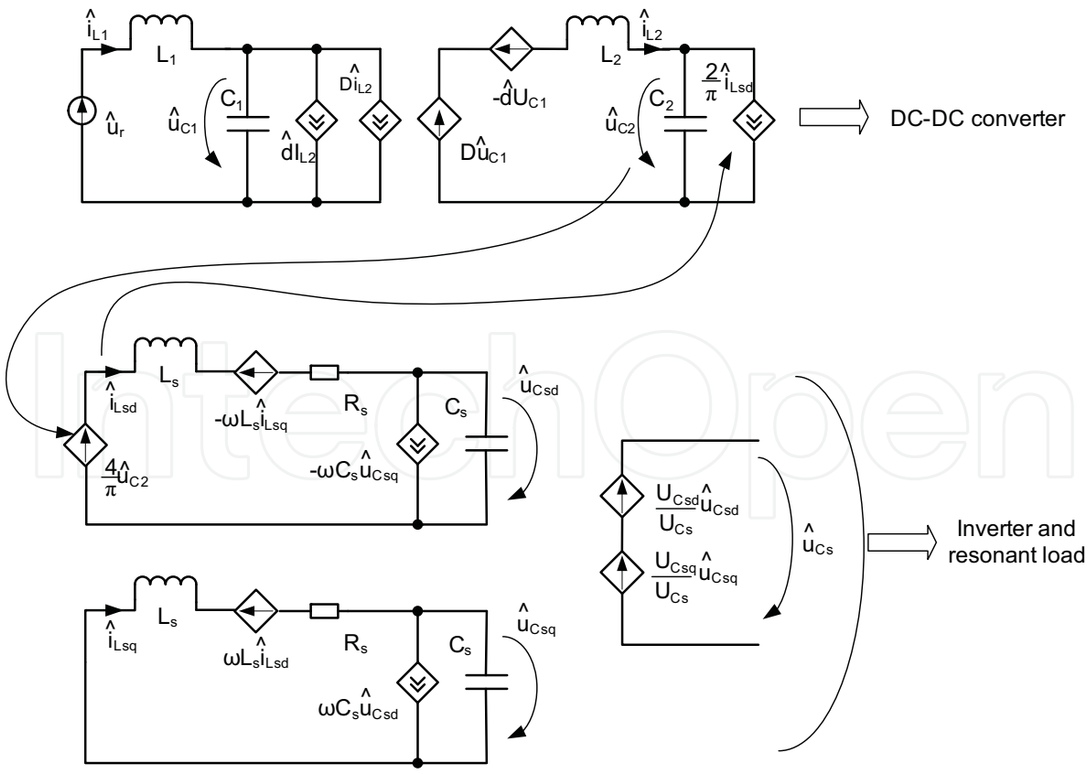

Fig. 15. The small-signal low-frequency model of the converter composed of filter, DC-DC converter, inverter and resonant load

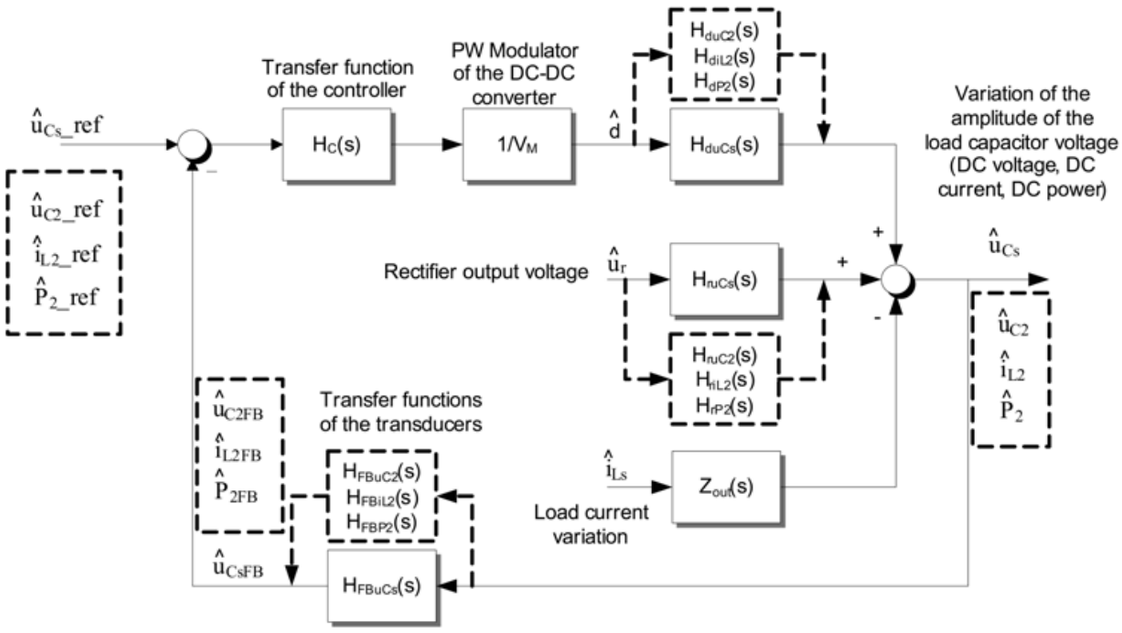

Fig. 16. Block diagram of the controlled converter

In Fig. 16 $H_{duCs}(s), H_{duC2}(s), H_{diL2}(s), H_{dP2}(s)$ represent the transfer functions between the small variation of the duty factor of the DC-DC converter control around its steady-state value D and the small variation of the load capacitor voltage, output voltage, current and power of the step-down converter around the steady-state values U_{Csmax}, U_{C2}, I_{L2}, and P_2.
In a similar way, $H_{ruCs}(s), H_{ruC2}(s), H_{riL2}(s), H_{rP2}(s)$ represent the small-signal transfer functions between the rectified voltage and the load capacitor voltage, output voltage current and power of the step-down converter. $H_{FBuCs}(s), H_{FBuC2}(s), H_{FBiL2}(s), H_{FBP2}(s)$ represent the transfer functions of the transducers used to measure the controlled variables. $Z_{out}(s)$ is the output impedance of the converter.

$$\hat{u}_{Cs} = \hat{u}_{Cs\_ref} \frac{1}{H_{FBuCs}(s)} \frac{T_{uCs}}{1+T_{uCs}} + \hat{u}_r(s) \frac{H_{ruCs}(s)}{1+T_{uCs}} - \hat{i}_{Ls} \frac{Z_{out}}{1+T_{uCs}}, \tag{20}$$

where the open-loop gain is:

$$T_{uCs} = H_{FBuCs}(s) H_c(s) H_{duCs}(s) / V_M. \tag{21}$$

In (21), $1/V_M$ denotes the gain of the PWM modulator, which is inversely proportional with the V_M amplitude of the carrier.
The model introduced above offers the possibility to analyze the behaviour of the induction-heating converter in case of "slow" variation of different quantities like the inverter operation frequency and the duty factor of the step-down converter. The envelope of different signals has such a slow variation and the controllers are designed to control these slow variations. In other words, the control of the resonant load voltage means the control of its RMS value or the control of its peak value, without caring for its oscillatory character during a switching cycle.

The "slow" or "low-frequency" model of the high-frequency converter is used to derive the frequency characteristics applied in classical controller design. For example, Fig. 17 and Fig. 18 present the Bode plots of the open voltage control loop in case of different operation frequencies of the inverter, respectively in case of different duty factors of the DC chopper control.

The circuit parameters and the operation conditions are:

$U_r = 500V, L_1 = 1.6mH, C_1 = 1850\mu F, L_2 = 800\mu H, C_2 = 200\mu F, L_s = 64\mu H, C_s = 39nF, R_s = 4\Omega.$

The transfer function of the voltage transducer is represented by a $1:5000$ gain. The gain of the PWM modulator is $V_M = 1$, while the parameters of the PI voltage controller are $K_p = 1, T_i = 1s$.

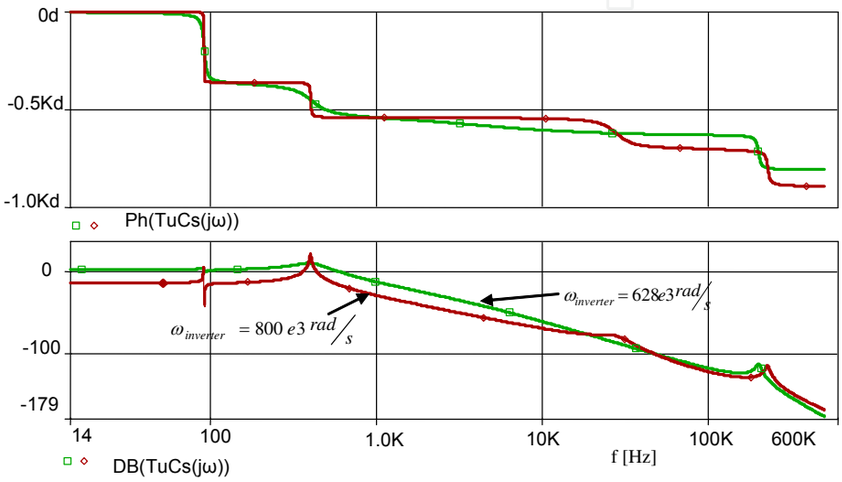

Fig. 17. Bode diagrams of the u_{Cs} voltage control loop for different inverter operation frequencies (ω = 800 krad/s and ω = 628 krad/s) in case of D=0.5

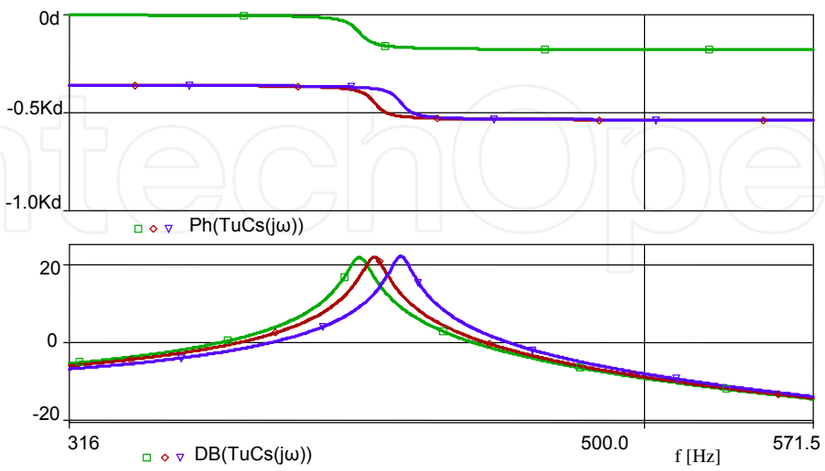

Fig. 18. Bode diagrams of the u_{Cs} control loop for different values of the step-down converter duty cycle: D = 0.2, D=0.5 and D=0.8, for ω = 800 krad/s

Keeping in mind that the control of the high frequency voltage is performed by means of the step-down DC-DC converter, i.e. by means of the variation of its control duty factor, it can be observed how the value of this duty factor and the value of the inverter operating frequency influence the frequency characteristics of the control loop.

5. Sampled-data modelling

The sampled-data models can be used for large-signal and small-signal analysis of the resonant converters.

The digital control of the converters is inherently based on sampled measurement data and discrete-time controller output.

Let's consider the classical thyristor-based, medium-frequency induction-heating converter from Fig. 19. This converter performs the power control by means of the controlled rectifier. The current inverter can operate only with a capacitive phase shift between the inverter output current and the resonant load voltage, as shown in Fig. 20, necessary for the recovery of the thyristors. The capacitive phase shift is controlled by a dedicated controller in a manner that positive AK voltage is applied to the thyristors only after the elapse of the circuit-commutated recovery time.

The presentation of the controllers which are able to guarantee this time delay between the end of the commutation period and the zero travel of the resonant capacitor voltage (see Fig. 20) is behind the scope of this chapter. Nevertheless, in order to develop a model which can be used for the power controller design, it is enough to assume that the problem is solved and this time delay is being controlled accurately by a control loop which is much faster than the power control loop. The result is the inverter operation at a frequency that assures the phase shift corresponding to the above condition. For a given resonant load the switching frequency can be determined using a fundamental-frequency approach. For instance, in case of the converter from Fig. 19, with the circuit parameters $L_d = 10\ mH$, $L_i = 10.14\ \mu H$, $R_i = 63.7\ m\Omega$, $C_p = 25\ \mu F$, the resonance frequency of the parallel resonant load is $f_0 = 10\ kHz$, and operation at $f_0 = 10.2\ kHz$ assures a $T_s = 7.5\ \mu s$ thyristor recovery time.

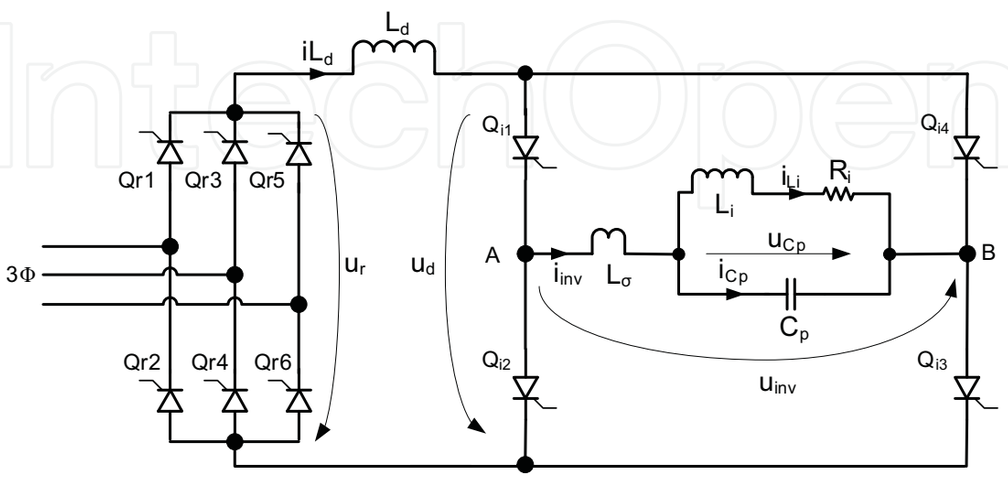

Fig. 19. Thyristor-based induction-heating converter with parallel resonant load

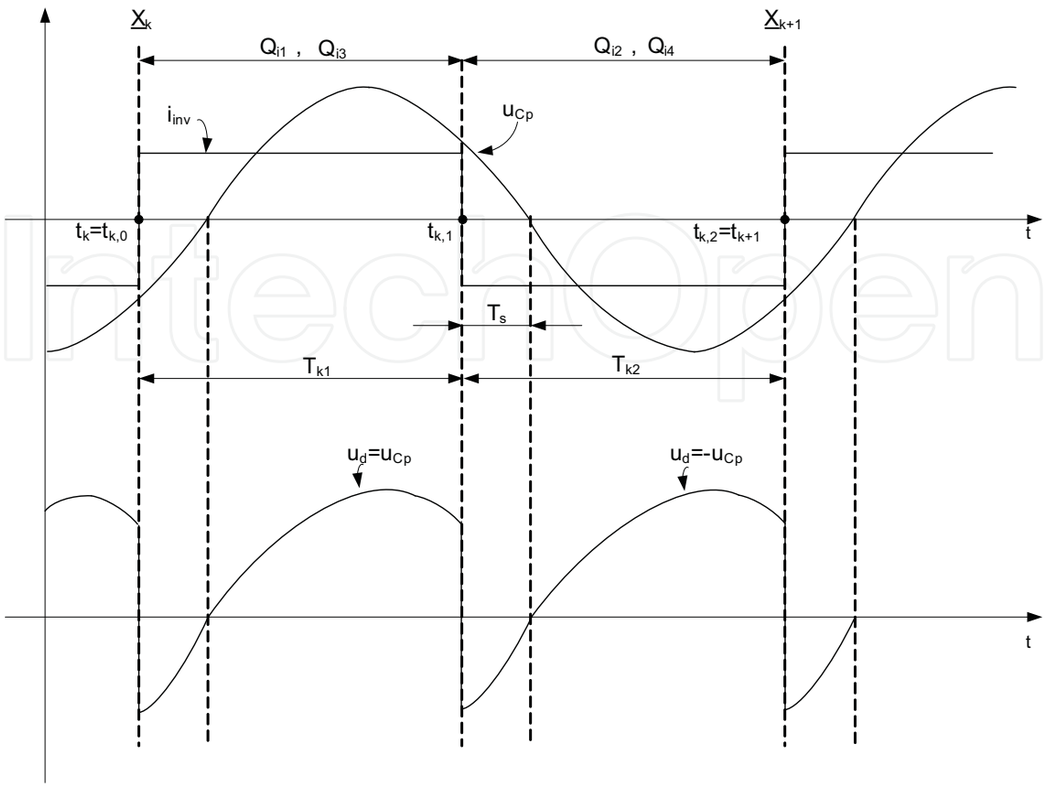

Fig. 20. Characteristic waveforms of the converter from Fig. 19

The above assumptions make possible the division of the switching period into time intervals with known lengths, corresponding to known switching states. This approach assumes the a priori knowledge of the converter operation and can be used only at a certain level of the hierarchical modelling.

As a simplifying assumption, the stray inductance L_σ is omitted. In consequence, the switching time is reduced to zero and only two states have to be considered corresponding to the conduction of the diagonals Q_{i1}, Q_{i3} and Q_{i2}, Q_{i4}.

The switching states of the converter are described by the equations (22). These equations form the state-space description of the linear time-invariant systems corresponding to the two switching states.

T_{ki} represents the i-th switching state of the *k*-th switching period.

A_i and B_i (23) represent the system matrices corresponding to the *i*-th switching state.

$$\begin{array}{ll} \textit{switching state } "T_{k1}" & \textit{switching state } "T_{k2}" \\ \begin{cases} \dfrac{di_{Ld}}{dt} = -\dfrac{1}{L_d}\cdot u_{Cp} + \dfrac{1}{L_d}\cdot u_r \\ \dfrac{di_{Li}}{dt} = -\dfrac{R_i}{L_i}\cdot i_{Li} + \dfrac{1}{L_i}\cdot u_{Cp} \\ \dfrac{du_{Cp}}{dt} = \dfrac{1}{C_p}\cdot i_{Ld} - \dfrac{1}{C_p}\cdot i_{Li} \end{cases} & \begin{cases} \dfrac{di_{Ld}}{dt} = \dfrac{1}{L_d}\cdot u_{Cp} + \dfrac{1}{L_d}\cdot u_r \\ \dfrac{di_{Li}}{dt} = -\dfrac{R_i}{L_i}\cdot i_{Li} + \dfrac{1}{L_i}\cdot u_{Cp} \\ \dfrac{du_{Cp}}{dt} = -\dfrac{1}{C_p}\cdot i_{Ld} - \dfrac{1}{C_p}\cdot i_{Li} \end{cases} \end{array} \quad (22)$$

$$A_1=\begin{bmatrix} 0 & 0 & -\frac{1}{L_d} \\ 0 & -\frac{R_i}{L_i} & \frac{1}{L_i} \\ \frac{1}{C_p} & -\frac{1}{C_p} & 0 \end{bmatrix},\quad B_1=\begin{bmatrix} \frac{1}{L_d} \\ 0 \\ 0 \end{bmatrix}\quad A_2=\begin{bmatrix} 0 & 0 & \frac{1}{L_d} \\ 0 & -\frac{R_i}{L_i} & \frac{1}{L_i} \\ -\frac{1}{C_p} & -\frac{1}{C_p} & 0 \end{bmatrix},\quad B_2=\begin{bmatrix} \frac{1}{L_d} \\ 0 \\ 0 \end{bmatrix} \tag{23}$$

$$\begin{cases} \dfrac{d\underline{x}(t)}{dt}=A_i\cdot\underline{x}(t)+B_i\cdot\underline{u}(t) & t\in(t_{k,i-1},t_{k,i}),\quad i=1,2 \\ \underline{x}(t)=\left[i_{Ld}(t)\quad i_{Li}(t)\quad u_{Cp}(t)\right]^T \end{cases}. \tag{24}$$

The state vector at the end of the *k*-th switching period denoted by $\underline{x}_{k+1}$ can be determined based on the state vector at the beginning of this period, denoted by $\underline{x}_k$.
According to the formulation from (Elbuluk et al., 1998),

$$\underline{x}(t_{k+1})=f\left(\underline{x}(t_k),P_k\right). \tag{25}$$

$P_k=\left[u_r\ L_d\ L_i\ R_i\ C_p\ t_{k,1}\ t_{k,2}\right]^T$ represents the vector of controlling parameters, including the controlled transition times defined by the thyristor firing instants.
A more accurate model should take into account also the commutation period characterized by the simultaneous conduction of the inverter thyristors. The end of this switching state is controlled "internally", i.e. it is not directly determined by the control system, but by the evolution of some circuit variables (i.e. by the zero transition of the thyristor currents). The internally controlled switching instants become parameters of (25), which forms a system of nonlinear equations together with the equations which formulate the conditions of these internally controlled transitions.
The state vector is continuous across the transitions between the switching states. In order to determine $\underline{x}_{k+1}$, the state transition matrix is built using the system matrices (23).
The state transition from $t_k=t_{k,0}$ to $t_{k,1}$ i.e. during the time interval T_{k1} is determined by the equation (26), where $u_r(t_k)$ represents the sampled (and held) value of the rectified voltage. In case of a 10 kHz medium-frequency induction-heating converter, this voltage has a slow variation (a 300 Hz component) in comparison with the switching frequency. Thus, the assumption that it is constant during a switching period is acceptable. In case of low-frequency converters this assumption is not valid any more and the steps must be refined.

$$\underline{x}(t_{k,1})=e^{A_1T_{k1}}\underline{x}(t_k)+\left(\int_0^{T_{k1}}e^{A_1\alpha}d\alpha\right)B_1u_r(t_k)=\Phi_1\underline{x}(t_k)+\Gamma_1u_r(t_k)=\Phi_1\underline{x}(t_k)+A_1^{-1}(\Phi_1-I)B_1u_r(t_k) \tag{26}$$

The state transition from $t_{k,1}$ to $t_{k+1}=t_{k,2}$ i.e. during the time interval T_{k2} can be described according to the relation (27).

$$\begin{aligned} &\underline{x}(t_{k+1})=e^{A_2T_{k2}}\underline{x}(t_{k,1})+\left(\int_0^{T_{k2}}e^{A_2\alpha}d\alpha\right)B_2u_r(t_k)=\Phi_2\underline{x}(t_{k,1})+\Gamma_2u_r(t_k)= \\ &=\Phi_2\underline{x}(t_{k,1})+A_2^{-1}(\Phi_2-I)B_2u_r(t_k) \end{aligned}. \tag{27}$$

By substitution of (26) into (27), it results:

$$\begin{aligned}\underline{x}(t_{k+1}) &= \Phi_2\left(\Phi_1\underline{x}(t_k) + A_1^{-1}(\Phi_1 - I)B_1u_r(t_k)\right) + A_2^{-1}(\Phi_2 - I)B_2u_r(t_k) = \\ &= \Phi_2\Phi_1\underline{x}(t_k) + \left(\Phi_2A_1^{-1}(\Phi_1 - I)B_1 + A_2^{-1}(\Phi_2 - I)B_2\right)u_r(t_k) = \Phi\underline{x}(t_k) + \Gamma u_r(t_k)\end{aligned} \quad . \tag{28}$$

Fig. 21, Fig. 22 and Fig. 23 show the results of sampled-data analysis superimposed with the results of a detailed circuit analysis performed using the Matlab- Simulink environment.
Fig. 21 demonstrates the transition of the state variable u_{Cp} between the starting instants of the switching periods.
Its sampled values are shown to be equal with the values of the continuous-time u_{Cp} in the moments of the $Q_{i2}, Q_{i3} \rightarrow Q_{i1}, Q_{i4}$ commutation , obtained by detailed analysis.

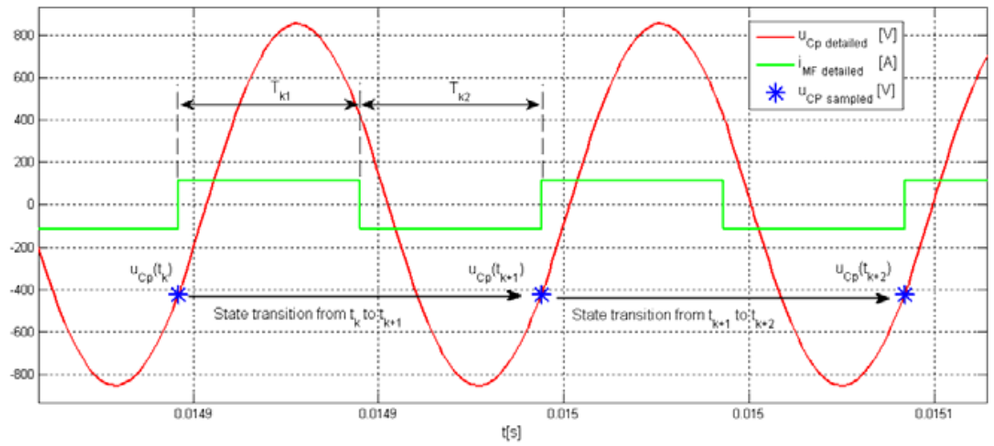

Fig. 21. The steady-state waveform of the resonant capacitor tank voltage obtained using the detailed model and the corresponding sampled-data result

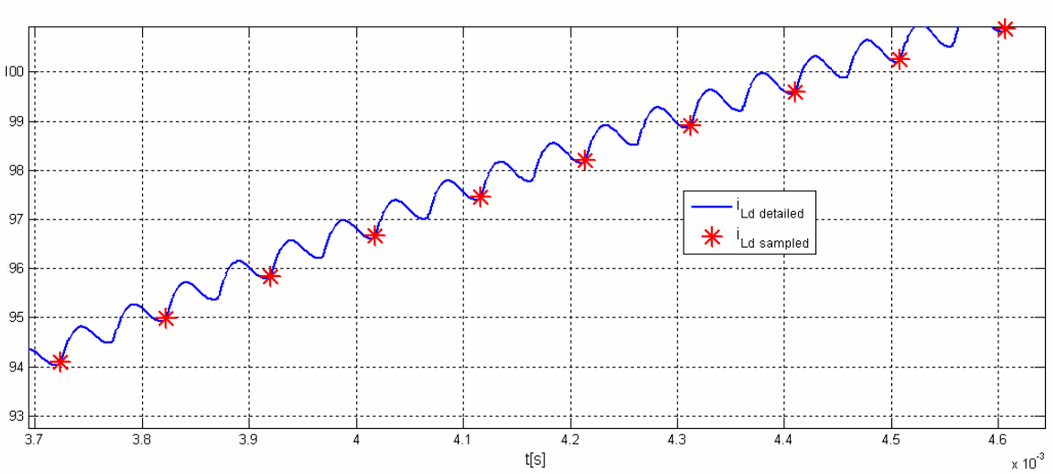

Fig. 22. The steady-state waveform of the DC-link current and the corresponding sampled-data result

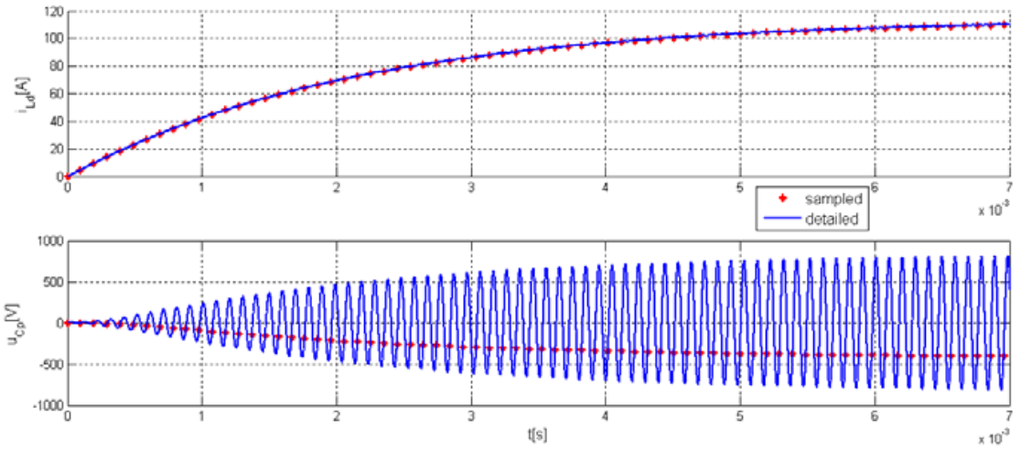

Fig. 23. Evolution of the DC-link current and of the capacitor voltage during the converter start-up

Fig. 22 and Fig. 23 demonstrate that i_{Ld} is a "slow" variable and that its evolution is described well enough by the sampled-data model.
Thus, the sampled-data modelling can be used for power controller design, resulting in a much shorter processing time, than the application of a detailed model.

6. Inverter analysis using the describing function method

The sinusoidal describing function method characterizes the output of the nonlinear part of a system by its fundamental component. If the output of the nonlinear part is fed to the input of a linear part of the system with low pass filter characteristics, the higher harmonic components are filtered out and the fundamental component approach would introduce only small errors.
The induction-heating inverters usually have a quasi-rectangular output voltage or current, which feeds a resonant load with good band-pass filter characteristics. This is the reason why most of the electrical quantities from the load can be considered sinusoidal.
That's why the describing function method can be introduced in a natural way for the analysis of the resonant converters (Sewell et al., 2004), (Kelemen & Kutasi, 2007b).
Let us consider the inverter circuit from Fig. 24., with lossless snubber capacitors and series resonant load modelled by a sinusoidal current source.
The describing function of the inverter output voltage is derived in order to represent its non-linear dependence on the inverter output current. The waveforms of the inverter output current and of the half-bridge voltage are shown in Fig. 25 in case of an optimal switching strategy characterized by the minimum value of the turn-off current that still assures zero voltage turn-on of the transistors.
The investigation is started from the moment when *Q3* is turned off. In the $(0...\gamma)$ interval, the *iLs* current flows through C_3 and C_4.
Assuming that $C_i = C$ and $u_{C3} + u_{C4} = U_d = ct.$, it results:

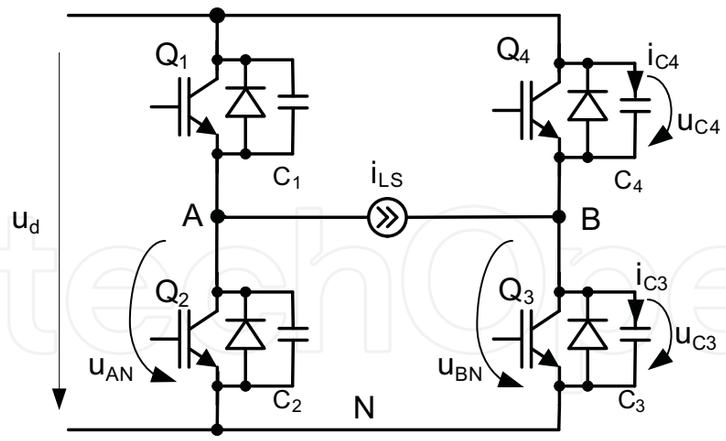

Fig. 24. Voltage-source inverter with snubber capacitors and the resonant load modelled by a current source

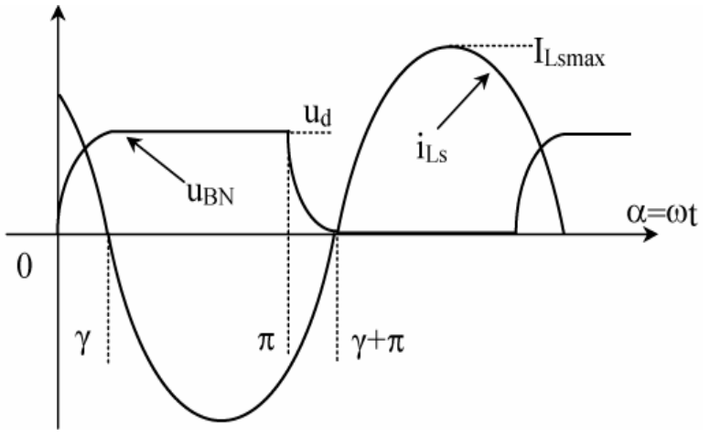

Fig. 25. The resonant load current and half-bridge voltage waveforms in case of optimal ZVS control of the inverter from Fig. 24

$$u_{BN}(\alpha)=\begin{cases}\dfrac{1}{2\omega C}\displaystyle\int_0^{\alpha}(-I_{Ls\max})\sin(\varphi-\gamma)d\varphi=\dfrac{I_{Ls\max}}{2\omega C}\left(\cos(\alpha-\gamma)-\cos\gamma\right) & for \quad \alpha\in(0,\gamma)\\ U_d+\left(\dfrac{I_{Ls\max}}{2\omega C}\left(\cos(\alpha-\gamma)+\cos\gamma\right)\right) & for \quad \alpha\in(\pi,\pi+\gamma)\\ 0 & for \quad \alpha\in(\pi+\gamma,2\pi)\end{cases}. \tag{29}$$

From the $u_{BN}(\gamma)=U_d$ condition,

$$\cos\gamma=1-\frac{2\omega CU_d}{I_{Ls\max}}. \tag{30}$$

The inverter output voltage is defined by the equations:

$$u_{AB}=\begin{cases} U_d-\dfrac{I_{Ls\max}}{\omega C}\left(\cos(\alpha-\gamma)-\cos\gamma\right) & \alpha\in(0,\gamma) \\ -U_d & \alpha\in(\gamma,\pi) \\ -U_d-\dfrac{I_{Ls\max}}{\omega C}\left(\cos(\alpha-\gamma)+\cos\gamma\right) & \alpha\in(\pi,\pi+\gamma) \\ +U_d & \alpha\in(\pi+\gamma,2\pi) \end{cases}. \tag{31}$$

The complex representation of the fundamental term of the inverter output voltage is:

$$\begin{gathered} \underline{u}_{AB1}=A_1e^{j\omega t}e^{j\left(-\frac{\pi}{2}+\varphi\right)}=\left(u_{AB1d}+ju_{AB1q}\right)e^{j\omega t},\ \text{where} \\ A_1=\sqrt{a_1^2+b_1^2},\quad a_1=\frac{2U_d}{\pi}\frac{\sin\gamma-\gamma\cos\gamma}{1-\cos\gamma},\quad b_1=\frac{2U_d}{\pi}\frac{(-\gamma\sin\gamma)}{1-\cos\gamma} \end{gathered} \tag{32}$$

The relationship between the inverter output voltage and the load current can be represented by the describing function defined as the ratio of the complex representations of their fundamental components:

$$N\left(I_{Ls\max},\omega\right)=\frac{\underline{u}_{AB1}}{\underline{i}_{Ls}}=\frac{2}{\pi}\frac{U_d}{I_{Ls\max}}\left(1+\cos\gamma+j\frac{\gamma-\sin\gamma\cos\gamma}{1-\cos\gamma}\right). \tag{33}$$

The phase shift between the fundamentals of the inverter output voltage and current is:

$$\varphi\left(\underline{u}_{AB1},\underline{i}_{Ls}\right)=\arg\left(N\left(I_{Ls\max},\omega\right)\right)\ \Rightarrow\ \varphi=arctg\frac{\gamma-\sin\gamma\cos\gamma}{\sin^2\gamma}. \tag{34}$$

Thus, the inverter can be seen as a system with the structure from Fig. 26.
One should bear in mind that the nonlinear relationship between the inverter output voltage and current results both from the existence of an intrinsic feedback loop due to the presence of the lossless snubber capacitors, and from the presence of the fast control loop of the switching angle γ.

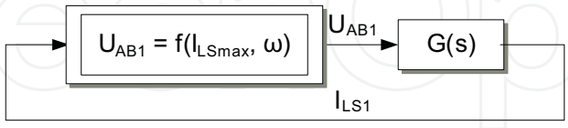

Fig. 26. System structure with nonlinear part represented by the describing function (31), and linear part represented by the linear resonant load

The existence of limit cycles in the optimal ZVS control mode can be verified using the describing function of the nonlinear part of the system and the transfer function of the serial load (35)

$$G(j\omega)=\frac{I_{Ls1\max}(j\omega)}{U_{AB1\max}(j\omega)}=\frac{j\omega C_s}{1-\omega^2C_sL_s+j\omega R_sC_s}, \tag{35}$$

where R_s, L_s, C_s denote the parameters of the serial resonant induction heating load.
The structure of the model of the PAM converter from Fig. 13, defined using the describing function of the inverter is shown in Fig. 27.

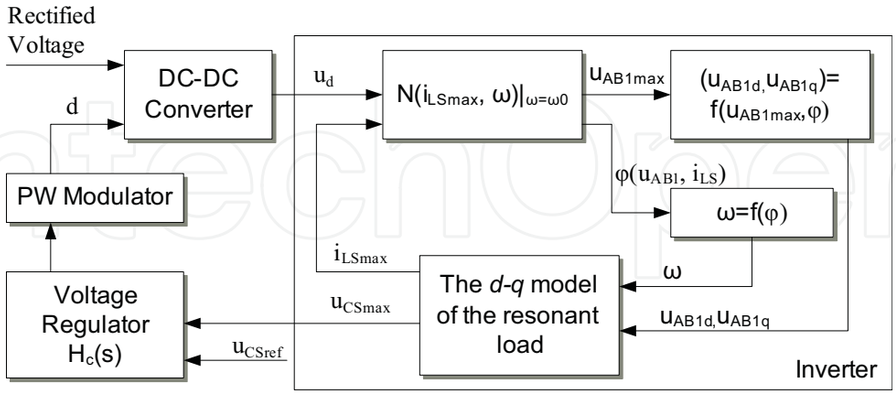

Fig. 27 Induction heating converter model with optimal (ZVS and close to ZCS) switching mode control of the inverter

The model from Fig. 26 encloses the *d-q* model of the resonant load (Kelemen & Kutasi, 2007a) and the model of the DC-DC converter obtained by the classical state-space averaging method.

7. Conclusion

Specific procedures have been presented that can be applied for modelling and analysis of the induction-heating power electronic converters. The basic idea behind this brief overview is that different tools have to be identified in order to handle the tasks arising at different hierarchical levels of the converter analysis.
Details have been presented in case of the methods that prove to be useful for system-level modelling. Thus, averaging and sampled-data modelling techniques have been applied in case of load-resonant transistor-based and thyristor-based inverters, taking into account the operating conditions imposed by the specific control tasks of these converters.
It has been shown that the describing function method is suitable for modelling of the nonlinearities in case of the inverters that operate close to the resonance frequency of the load.
The presented procedures have been used for development of several induction-heating equipments in the frequency range of $50\ Hz \div 500\ kHz$ and in power range of $4 \div 1000\ kW$.

8. References

Borelli, F. (2003). *Constrained Optimal Control of Linear and hybrid Systems*, Springer Verlag, ISBN: 3-540-00257-X, Berlin, Heidelberg

Elbuluk, M. E., Verghese G. C. & Kassakian, J.G. (1998). Sampled-data modeling and digital control of resonant converters, *IEEE Transactions on Power Electronics*, Vol. 3, No. 3, July 1988, 344–354, ISSN: 0885-8993

Erickson, R. W. & Maksimović, D. (2004). *Fundamentals of power electronics- second edition*, Kluwer Academic Publishers, Norwell, Massachusetts, ISBN: 0-7923-7270-0

Fischer, G. L. & Doht, H. C. (1994). An inverter system for inductive tube welding utilizing resonance transformation, *Proceedings of the Industry Applications Society Annual Meeting*, pp. 833–840 Vol. 2, ISBN: 0-7803-1993-1, Denver, CO, October 1994

Forest, F., Labouré, E., Costa, F. & Gaspard, J. Y. (2000). Principle of a multi-load/single converter system for low power induction heating, *IEEE Transactions on Power Electronics*, Vol. 15, No. 2, March 2000, 223-230, ISSN: 0885-8993

Foster, P. F., Sewell H. I., Bingham C. M., Stone D. A., Hente, D. & Howe D. (2003). Cyclic-averaging for high-speed analysis of resonant converters, *IEEE Transactions on Power Electronics*, Vol. 18, No. 4, July 2003, 985–993, ISSN: 0885-8993

Fujita, H. & Akagi, H. (1996). Pulse-density-modulated power control of a 4 kW, 450 kHz voltage-source inverter for induction melting applications, *IEEE Transactions on Industry Applications*, Vol. 32, No. 2, March/April 1996, 279-286, ISSN: 0093-9994

Kelemen, A. (2007). *Power control of the induction-heating power-electronic converters- PhD thesis*, Transylvania University of Brasov

Kelemen, A. & Kutasi, N. (2007a). Induction-heating voltage inverter with hybrid LLC resonant load, the D-Q model, *Pollack Periodica*, Vol. 2, No. 1, 2007, 27–37, ISSN: 1788-1994

Kelemen, A. & Kutasi, N. (2007b). Describing function analysis of a voltage-source induction-heating inverter with pulse amplitude modulation, *Acta Electrotehnica*, Vol. 48, No. 3, 2007, 223-229, ISSN 1841-3323

Krein, P. T., Bentsman, J., Bass, R. M. & Lesieutre, B. C. (1990) On the use of averaging for the analysis of power electronic systems, *IEEE Transactions on Power Electronics*, Vol. 5, No. 2, April 1990, 182-190, ISSN: 0885-8993

Mohan, N., Undeland, T. M. & Robbins, W. P. (2002). *Power Electronics - Converters, Applications and Design, 3rd edition*, John Wiley & Sons INC., New York, ISBN: 978-0-471-22693-2

Rim, C.T. & Cho, G. H. (1990) Phasor transformation and its application to the DC/AC analysis of frequency-phase-controlled series resonant converters (SRC), *IEEE Transactions on Power Electronics*, Vol. 5, No. 2, April 1990, 201–211, ISSN: 0885-8993

Rudnev, V., Loveless, D, Cook, R. & Black, M. (2003). *Handbook of induction heating*, Marcel Dekker, Inc., New York, Basel, ISBN: 0-8247-0848-2

Sanders, S. R., Noworolski, J. M., Liu, X. Z. & Verghese, G. C. (1991). Generalized averaging method for power conversion circuits, *IEEE Transactions on Power Electronics*, Vol. 6, No. 2, April 1991, 251–259, ISSN: 0885-8993

Sewell, H. I., Stone, D. A. & Bingham, C. M. (2004). A describing function for resonantly commutated H-bridge inverters, *IEEE Transactions on Power Electronics* ,Vol. 19, No. 4, July 2004, 1010-1021, ISSN: 0885-8993

Sluhotkii, A. E. & Rîskin, S. E. (1982) *Inductoare pentru încălzirea electrică* , Editura Tehnică, Bucureşti

Torrisi, F. D. & Bemporad, A. (2004). HYSDEL — A Tool for Generating Computational Hybrid Models for Analysis and Synthesis Problems, *IEEE Transactions on Control Systems Technology*, Vol. 12, No. 2, March 2004, 235–249, ISSN: 1063-6536

Zhang, Y. & Sen, P. C. (2004). D-Q models for resonant converters, *Proceedings of the 35th Annual IEEE Power Electronics Specialists Conference PESC 04*, pp. 1749–1753, Aachen, Germany, November 2004, ISBN: 0-7803-8399-0

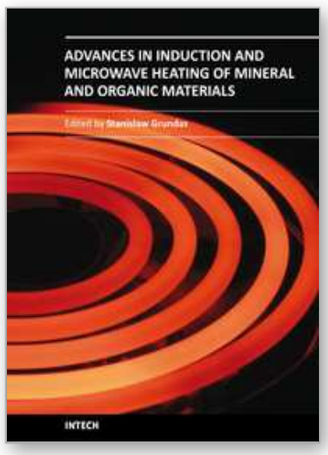

Advances in Induction and Microwave Heating of Mineral and Organic Materials

Edited by Prof. StanisÅ‚aw Grundas

ISBN 978-953-307-522-8
Hard cover, 752 pages
Publisher InTech
Published online 14, February, 2011
Published in print edition February, 2011

The book offers comprehensive coverage of the broad range of scientific knowledge in the fields of advances in induction and microwave heating of mineral and organic materials. Beginning with industry application in many areas of practical application to mineral materials and ending with raw materials of agriculture origin the authors, specialists in different scientific area, present their results in the two sections: Section 1-Induction and Microwave Heating of Mineral Materials, and Section 2-Microwave Heating of Organic Materials.

How to reference

In order to correctly reference this scholarly work, feel free to copy and paste the following:

András Kelemen and Nimród Kutasi (2011). Modeling and Analysis of Induction Heating Converters, Advances in Induction and Microwave Heating of Mineral and Organic Materials, Prof. StanisÅ‚aw Grundas (Ed.), ISBN: 978-953-307-522-8, InTech, Available from: http://www.intechopen.com/books/advances-in-induction-and-microwave-heating-of-mineral-and-organic-materials/modeling-and-analysis-of-induction-heating-converters

INTECH
open science | open minds

InTech Europe
University Campus STeP Ri
Slavka Krautzeka 83/A
51000 Rijeka, Croatia
Phone: +385 (51) 770 447
Fax: +385 (51) 686 166
www.intechopen.com

InTech China
Unit 405, Office Block, Hotel Equatorial Shanghai
No.65, Yan An Road (West), Shanghai, 200040, China
中国上海市延安西路65号上海国际贵都大饭店办公楼405单元
Phone: +86-21-62489820
Fax: +86-21-62489821

IntechOpen